Journal of Modern Optics

ISSN: 0950-0340 (Print) 1362-3044 (Online) Journal homepage: https://www.tandfonline.com/loi/tmop20

Nonlinear dynamics of coupled transverse modes in quantum cascade lasers

Aleksander K. Wójcik , Nanfang Yu , Laurent Diehl , Federico Capasso & Alexey Belyanin

To cite this article: Aleksander K. Wójcik , Nanfang Yu , Laurent Diehl , Federico Capasso & Alexey Belyanin (2010) Nonlinear dynamics of coupled transverse modes in quantum cascade lasers, Journal of Modern Optics, 57:19, 1892-1899, DOI: 10.1080/09500340.2010.506013

To link to this article: https://doi.org/10.1080/09500340.2010.506013

Published online: 11 Aug 2010.

Journal of Modern Optics
Vol. 57, No. 19, 10 November 2010, 1892–1899

Taylor & Francis
Taylor & Francis Group

Nonlinear dynamics of coupled transverse modes in quantum cascade lasers

Aleksander K. Wójcik[a]*, Nanfang Yu[b], Laurent Diehl[b], Federico Capasso[b] and Alexey Belyanin[a]

[a]*Department of Physics, Texas A&M University, College Station, TX 77843 USA;* [b]*School of Engineering and Applied Sciences, Harvard University, Cambridge, MA 02138 USA*

(*Received 16 March 2010; final version received 28 June 2010*)

We analyze the dynamics of broad-area mid-infrared quantum cascade lasers (QCLs). We show the possibility of the coherent coupling of several transverse modes which results in several interesting effects including frequency and phase locking between transverse modes, bistability, and beam steering. We present an analytical model for the modal dynamics and its numerical analysis. Effects of amplitude and phase fluctuations on the modal stability are explored. We compare our theoretical results with our experimental measurements of buried heterostructure QCLs.

Keywords: nonlinear optics; quantum cascade lasers; mode locking; beam steering

1. Introduction

Higher order transverse modes are routinely observed in quantum cascade lasers (QCLs) with waveguide widths exceeding 3–4 laser wavelengths in a medium. The transverse modes interact with each other through the inhomogeneous saturation of the active region (spatial hole burning effect). In certain cases this nonlinear interaction can prevail over the waveguide dispersion and result in phase and frequency locking of the modes.

Transverse mode effects in lasers have been the subject of extensive research over several decades. Dynamical transverse laser pattern formation has been studied in the context of laser instabilities [1,2], structured light [3], transverse pattern formation and control [4,5] and solitons [6]. For a review of work dating before the 1990s, see Abraham et al. [7] and references therein. Limited work on the subject has been done on QCLs. One possible signature of the transverse mode coherence in QCLs is the asymmetry in the near and far field of a laser beam, observed, for example, in [8–10]. QCLs operating in the mid-infrared range have the advantage of having a longer wavelength, which allows the fabrication of subwavelength metallic or dielectric pattern on the laser cavity, resulting in the radiation pattern control and plasmonic beam shaping, see e.g. [11] for a review. This combined with multi-transverse mode operation can result in dynamic light structures and selective transverse mode control.

In recent work [10] we have shown that the observed axial asymmetry and beam steering of the radiated field in QCLs is a manifestation of phase coherence between several lateral modes. The phase locking between different lateral modes can be explained through four-wave mixing utilizing resonant third-order ($\chi^{(3)}$) optical nonlinearity in the active region originated from inhomogeneous gain saturation. The mechanisms that govern nonlinear mode coupling in QCLs differ considerably from those in diode lasers, where multi-transverse mode behavior has been previously observed and analyzed [12]. QCLs have ultrafast gain recovery time of the order of 1 ps [13]. This timescale is much shorter than the cavity roundtrip time and the photon lifetime. Therefore, QCLs should demonstrate class-A laser behavior [14], accompanied by weak carrier diffusion and strong hole burning effects, as opposed to diode lasers that show class-B dynamics, strong carrier diffusion, and weak spectral and spatial hole burning.

Although thermal effects can lead to a temperature-dependent refractive index and far-field distortion, they do not lead to modal coherence and comb synchronization. Our experimental results and Fourier analysis of the laser spectra confirmed the presence of these two effects in the analyzed lasers. The observed coherent coupling of three transverse modes can only be explained by their nonlinear mixing, in fact, four-wave mixing.

In the present article we derive a model for the dynamics of the transverse modes in QCLs. The material gain is modelled as a two level medium, resulting in Maxwell–Bloch equations. The polarization and population variables are eliminated

*Corresponding author. Email: awojcik@physics.tamu.edu

ISSN 0950–0340 print/ISSN 1362–3044 online

DOI: 10.1080/09500340.2010.506013
http://www.informaworld.com

adiabatically (class-A laser), resulting in a system of nonlinear differential equations for complex amplitudes of cavity modes, to which amplitude and phase fluctuations are added phenomenologically. The equations are solved numerically in time domain, and the dynamics of the modes is systematically studied as a function of laser parameters: gain, losses, frequency detunings, etc. Our analysis is compared with experimental results for buried heterostructure QCLs. The results can be used to understand and control the effects of phase locking, beam steering, and pulsed operation in the mid-infrared range.

2. Equations of motion

Our analysis starts with a set of two-level Maxwell–Bloch equations, in which we perform modal decomposition of the electric field into cavity modes and the adiabatic elimination of the population inversion and coherence. The final derivation leads to a system of coupled nonlinear equations for complex amplitudes of the cavity modes.

Starting with Maxwell's equations, we decompose the electric field in the cavity into a sum of quasi-orthogonal waveguide modes:

$$\boldsymbol{E} = \sum_i e_i(t,z)\boldsymbol{E}_i(\boldsymbol{r}_\perp), \tag{1}$$

where $\boldsymbol{r}_\perp$ is the radius vector in the cross-section of the waveguide and z is the coordinate along the cavity. We have assumed that it is possible to separate the transverse and longitudinal field dependence. The transverse profile of the electric field $\boldsymbol{E}_i(\boldsymbol{r}_\perp)$ is the eigenmode solution of Maxwell's equations for a 2D laser waveguide. We introduce slowly varying complex amplitudes of the electric field:

$$e_i = \frac{1}{2}\left[a_i \exp(-\mathrm{i}\omega_0 t + \mathrm{i}\beta_i z) + a_i^* \exp(\mathrm{i}\omega_0 t - \mathrm{i}\beta_i z)\right], \tag{2}$$

where ω_0 is the laser transition frequency and β_i is the propagation constant of the ith mode.

The active region is modelled using density matrix equations for a two-level medium, with optical polarization expressed through a slowly varying amplitude σ of the off-diagonal element of the density matrix as

$$P = Nd[\sigma \exp(-\mathrm{i}\omega_0 t) + \sigma^* \exp(\mathrm{i}\omega_0 t)]. \tag{3}$$

By integrating Maxwell's equations over the cross-section A_T of the waveguide, making use of the orthogonality of the modes, and eliminating the fast oscillating terms (rotating wave approximation), we obtain

$$\frac{\partial \sigma}{\partial t} + \gamma_\perp \sigma = -\frac{\mathrm{i}d}{2\hbar} D \sum_i E_i a_i, \tag{4}$$

$$\frac{\partial D}{\partial t} + \gamma_\parallel (D - D_\mathrm{p}) = -\frac{\mathrm{i}d}{\hbar} \sum_i (a_i^* \sigma - a_i \sigma^*), \tag{5}$$

$$\frac{\partial a_i}{\partial t} + \frac{c}{\mu_i}\frac{\partial a_i}{\partial z} + (\kappa_i + \mathrm{i}\Delta_{ci}) a_i = \frac{4\pi \mathrm{i}\omega_0 N d}{\mu_i A_T} \int_{AR} \sigma E_i \,\mathrm{d}A \tag{6}$$

where N is the total electron density in the active region, d is the dipole moment of the laser transition, Δ_{ci} is the detuning of the ith mode from the central frequency ω_0, μ_i is the modal refractive index, $\gamma_\perp^{-1}$ and $\gamma_\parallel^{-1}$ are relaxation times for coherence and population inversion, respectively, and D_p is the population inversion supported by pumping in the absence of laser generation.

The relaxation times in QCLs are faster than photon decay times, which allows us to do adiabatic elimination of the polarization $\mathrm{d}\sigma/\mathrm{d}t = 0$ and population $\mathrm{d}D/\mathrm{d}t = 0$. We expand the polarization term in series and retain only the first two terms ($\chi^{(3)}$ approximation). Since we have a large number of longitudinal modes per one lateral mode as seen in the experimental spectra below, we employ the mean-field approximation by averaging the last equation over z and including mirror losses into waveguide losses κ_i. The equation of motion for the ith mode becomes as follows:

$$\frac{\mathrm{d}a_i}{\mathrm{d}t} + (\kappa_i + \mathrm{i}\Delta_{ci}) a_i = g\Gamma_i a_i - \frac{g}{I_\mathrm{S}} \sum_{j,k,l} a_j a_k^* a_l G_{ijkl}, \tag{7}$$

where the material gain and saturation intensity are defined by

$$g = \frac{4\pi\omega_0 N d^2 D_\mathrm{p}}{2\gamma_\perp \hbar \mu_i}, \quad I_\mathrm{S} = \frac{\hbar^2 \gamma_\parallel \gamma_\perp}{d^2}. \tag{8}$$

Here the overlap integrals are defined as

$$\Gamma_i = \frac{\int_{AR} \varepsilon E_i^2 \,\mathrm{d}A}{\int_{A_T} \varepsilon E_i^2 \,\mathrm{d}A}, \quad O_i = \frac{1}{A_T} \int_{AR} \varepsilon E_i^2 \,\mathrm{d}A, \tag{9}$$

$$G_{ijkl} = \frac{1}{A_T (O_i O_j O_k O_l)^{1/2}} \int_{AR} \varepsilon E_i E_j E_k E_l \,\mathrm{d}A \tag{10}$$

where AR is the cross-sectional area of the active region. The factors G_{ijkl} are symmetric with respect to any permutation of the sub-indices, which is clear from the definition (Equation (10)). The symmetry simplifies the numerical calculations.

As the final step we add phenomenologically a noise term to the equations. Since the QCLs are

class-A lasers, noise analysis differs from that of standard semiconductor lasers and it gets more complicated by the correlation of photons through the reuse of electrons while they travel inside the cavity. The specifics of noise correlation effects are discussed in the literature [15,16].

Our numerical analysis showed that fluctuations in the injection current do not influence the basic behavior of the modes and we will neglect it, concentrating on fluctuations of the complex amplitudes of the modes. One possible source of these fluctuations is the spontaneous emission.

The noise enters our equations as an extra equation, with a stochastic source term added to the complex field amplitude,

$$a_i(t) \rightarrow a_i(t) + \tilde{a}\xi_i(t). \tag{11}$$

The noise term has the following characteristics:

$$\begin{aligned} \langle \xi_i(t) \rangle &= 0, \\ |\langle \xi_i(t)\xi_j(t') \rangle| &= \delta_{ij}\delta(t-t'). \end{aligned} \tag{12}$$

Here $\tilde{a}$ is the noise amplitude and $\xi(t)$ is a stochastic process, with a complex uniform distribution function and $0 \leq |\xi(t)| \leq 1$.

3. Numerical modeling

We solve the resulting system of coupled nonlinear differential equations (Equations (7)) numerically. The initial conditions for the amplitudes are taken as a set of randomly distributed complex amplitudes, with magnitudes of the order of 10^{-3}. This accounts for the amplification of the cold cavity modes from spontaneous emission. The equations are integrated until the amplitudes reach either steady state or a periodic form.

An example of the dynamics of three transverse modes is presented in Figure 1. The modes are the TM_{00}, TM_{01} and TM_{02} modes. The transverse distributions, losses, frequencies, and propagation constants of cold waveguide modes were found with COMSOL software using the Finite Element Method and were consequently used to find the overlap integrals G and Γ. The laser geometry corresponded to buried heterostructure lasers shown in the experimental section below. Details of the mode calculation methodology can be found in [17]. The values of parameters used for the simulations are presented in Table 1. The gain g_{th} is the threshold gain for the TM_{01} mode which has the lowest threshold.

Next, we find stable steady state solutions by solving Equations (7) starting from a large set of random initial conditions and following the modal evolution with time until the stable solution is reached.

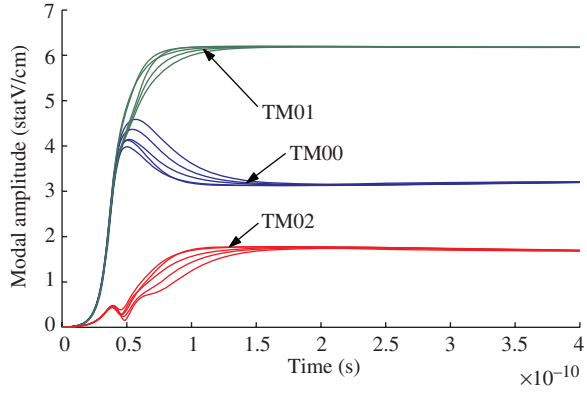

Figure 1. Time-dependent dynamics of modal amplitudes for five random initial conditions. The gain is 3.5 times g_{th}. (The color version of this figure is included in the online version of the journal.)

Table 1. Parameters and modes used in the simulations.

Mode	TM_{00}	TM_{01}	TM_{02}
Δ_{ci} (rad s^{-1})	-6.52×10^{10}	0	6.29×10^{10}
κ_i (rad s^{-1})	7.86×10^{10}	6.82×10^{10}	9.08×10^{10}
Γ	0.517	0.496	0.448
I_S (erg s^{-1} cm^{-2})		1.205×10^{3}	
$\tilde{a}$ (statV cm^{-1})		1×10^{-2}	
g_{th} (rad s^{-1})		1.37×10^{11}	

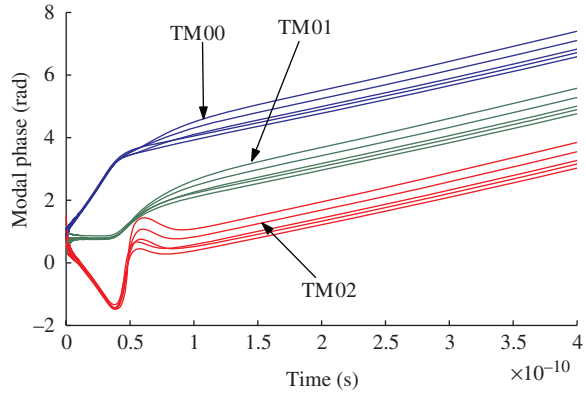

Figure 2. Phases corresponding to the same simulations as in Figure 1. (The color version of this figure is included in the online version of the journal.)

An example of such analysis is shown in Figure 1 for the amplitudes and Figure 2 for the phases of complex amplitudes a_i. The nonlinear interaction leads to frequency pulling, merging the transverse modes into a single frequency with a constant phase difference between them. This can be observed from Figure 2 as

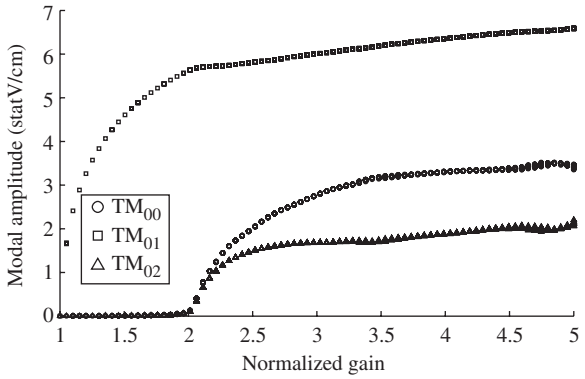

Figure 3. Amplitudes of the modes as a function of gain, normalized to g_{th}. All three modes are present.

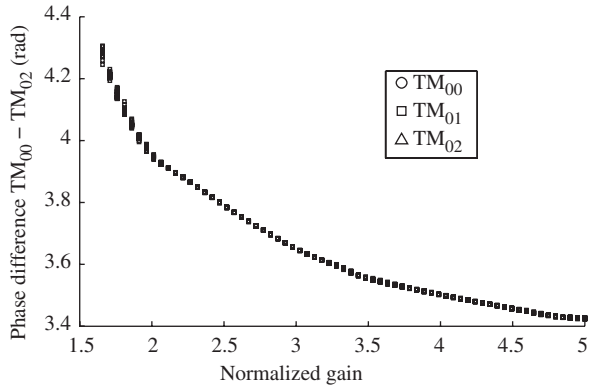

Figure 5. Phases of the modes as a function of gain, normalized to g_{th}. The phase relation between the modes is a function of gain, resulting in beam steering of the field.

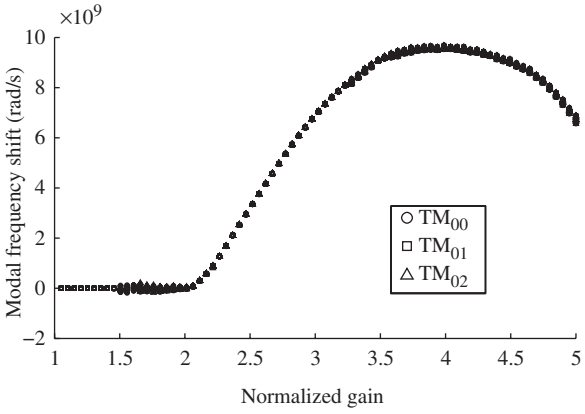

Figure 4. Frequencies of the modes as a function of gain, normalized to g_{th}. The modes lock to a single frequency.

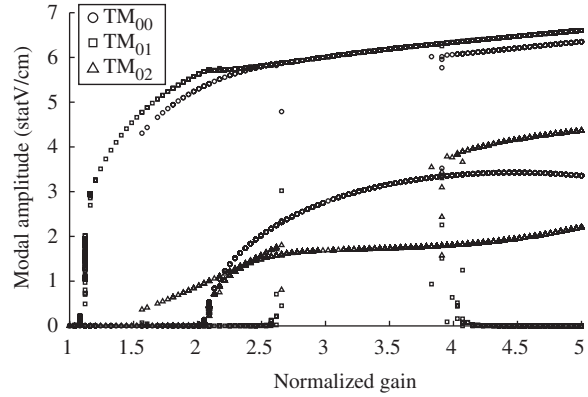

Figure 6. Bistability in modal amplitudes as a function of gain, normalized to g_{th}.

well, where the slope of the phase is the frequency. Experimentally this effect should lead to merging of three combs belonging to different transverse modes into a single comb, while the far-field pattern shows the presence of all three transverse modes with locked phases. The phase difference between the modes determines the exact form and the amount of the beam steering in the far field. This behavior is in fact observed as we discuss below.

The same time-dependent simulations starting from a random set of initial conditions were made for a broad range of gain values. The values of the parameters were the same as previously, only the parameter g was varied. The results are plotted in Figures 3 and 4, where the gain is normalized to the value g_{th} from Table 1.

The three modes lock to a single frequency, forming a gain-dependent far-field pattern. The dominant mode TM_{01} starts lasing with a normalized gain of 1, while the other two modes appear almost simultaneously when the gain is two times higher, as seen from Figure 4. The relative phase of the modes also depends on the gain, varying almost monotonously, as presented in Figure 5. This figure shows only the phase relation between modes TM_{00} and TM_{02} at the final time of the simulation. This phase dependence of the gain, determines the exact angular distribution of the pump-dependent asymmetric beam pattern.

We extend our analysis to the case where noise becomes negligible, which in our case represents taking the noise amplitude below approximately $\tilde{a} < 1 \times 10^{-3}$ statV cm^{-1}. In this case the laser shows a bistability behavior. The amplitudes of steady state solutions from a time dependent simulation are shown in Figure 6. The simulation is repeated for the same value of gain, but randomly taking another set of initial conditions. The final amplitude takes one of the two branches depending of the initial condition – the effect that did not exist when the noise was an order of magnitude higher. All transverse modes lock to the

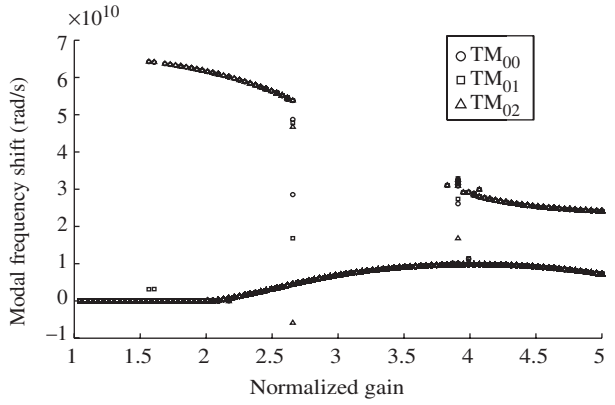

Figure 7. Frequencies of all three modes lock to two different frequencies, normalized to g_{th}.

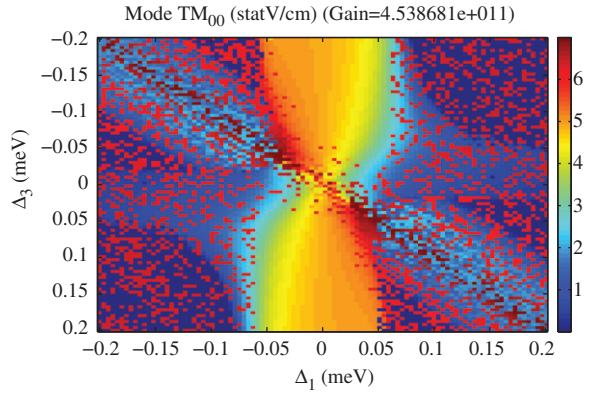

Figure 8. The amplitudes of mode TM_{00} as a function of Δ. (The color version of this figure is included in the online version of the journal.)

same frequency, but this frequency is different for each of the bistable states, as shown in Figure 7.

Interestingly, there exists an intermediate range of gains where only one stable steady state solution exists, as shown in Figures 6 and 7. The two boundaries of this region are points of bifurcations where the second solution appears. In the immediate vicinity of each boundary, there is an unstable region where multiple solutions exist depending on the initial conditions and the level of noise. In this region the laser is expected to randomly hop between different mode patterns.

The coexistence of two stable solutions may seem puzzling, but close inspection of Figure 6 reveals that the second stable solution contains only two lateral modes – the third mode has zero amplitude. The latter mode is actually the TM_{01} mode which has the lowest threshold and starts lasing first when the pump is turned on; therefore its suppression and the emergence of the second, two-mode solution is entirely due to a strong nonlinear interaction and competition between modes.

The bistability effect is not strongly dependent on the spectral separation between the cold waveguide modes, or Δ parameters in our model. We explored the dependence of the modal amplitude on a Δ plane, and observed that the bistability is fairly independent of Δ_3 and needs a certain threshold for $\Delta_{1,th} < \Delta_1$ to appear, as can be seen from Figures 8 and 9. In the case analyzed here, $\Delta_{1,th} \simeq 0.05$ meV. The amplitude of the mode TM_{00} is different from 0, independently of Δ_3 as long as Δ_1 is below 0.05 meV. The same case follows for mode TM_{02}, as long as Δ_3 is below 0.05 meV.

The actual separation of the lateral modes depends directly on the shape of the cavity and the design of the QCLs. A more detailed experimental study of the spectral distribution of the cavity modes has been performed by Stelmakh et al. [18]. He found a broad

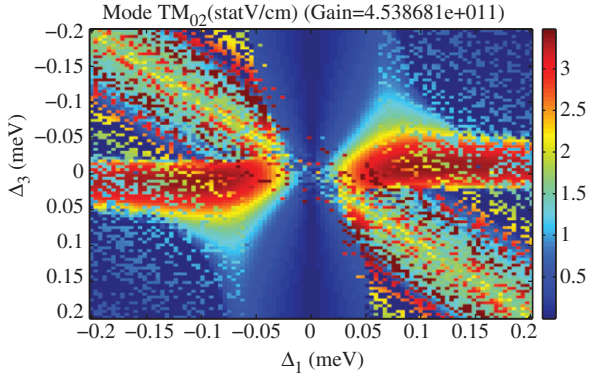

Figure 9. The amplitudes of mode TM_{02} as a function of Δ. (The color version of this figure is included in the online version of the journal.)

range of values for spectral separation between lateral modes, from a nearly degenerate case of merging lateral modes to fairly large separation of the order of the distance between neighboring longitudinal modes (about 0.1 meV for a 2 mm long cavity). Spectral position of cold cavity modes is an important design and optimization parameter for the control of the nonlinear transverse mode dynamics.

The stable steady-state solutions found with the time-dependent analysis can be compared with a set of *all* frequency- and phase-locked steady-state solutions that can be obtained by eliminating time derivatives from the equations and solving for only the steady-state solutions. By changing the complex field variables into phases and amplitudes, we look for constant-amplitude, steady-state solutions of the form

$$a_j(t) = f_j \exp(i\Omega t + i\phi_j). \tag{13}$$

The amplitudes and phases f_j and ϕ_j become time independent and the modes lock to a single frequency Ω. The system of equations has one more unknown than the resulting number of equations. In this case it is possible to set one of the phases, $\phi_j = 0$, without loss of generality, and eliminate one of the variables. The steady-state system of equations takes the following form,

$$\kappa_j f_j - g\Gamma_j f_j = \frac{-2g}{Is}\sum_{k,l,m} G_{jklm} f_k f_l f_m \cos\phi_{jklm},$$

$$\Omega f_j + \Delta_j f_j = \frac{-2g}{Is}\sum_{k,l,m} G_{jklm} f_k f_l f_m \sin\phi_{jklm},$$

$$\phi_{jklm} = \phi_k + \phi_l - \phi_m - \phi_j. \tag{14}$$

In our case we take $\phi_2 = 0$. The solutions for the TM_{01} mode are presented in Figure 10.

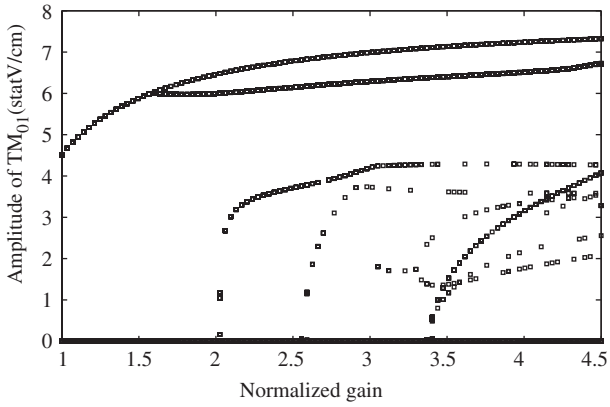

Figure 10. Steady state solutions as a function of gain for the mode TM_{01}.

Both states from the bistability regime are present among all steady state-solutions. The change from the bistable to stable regime is accompanied by the change in the total number of steady-state solutions.

4. Experimental results

An experimental example of such frequency- and phase-locked behavior is presented in Figure 11,

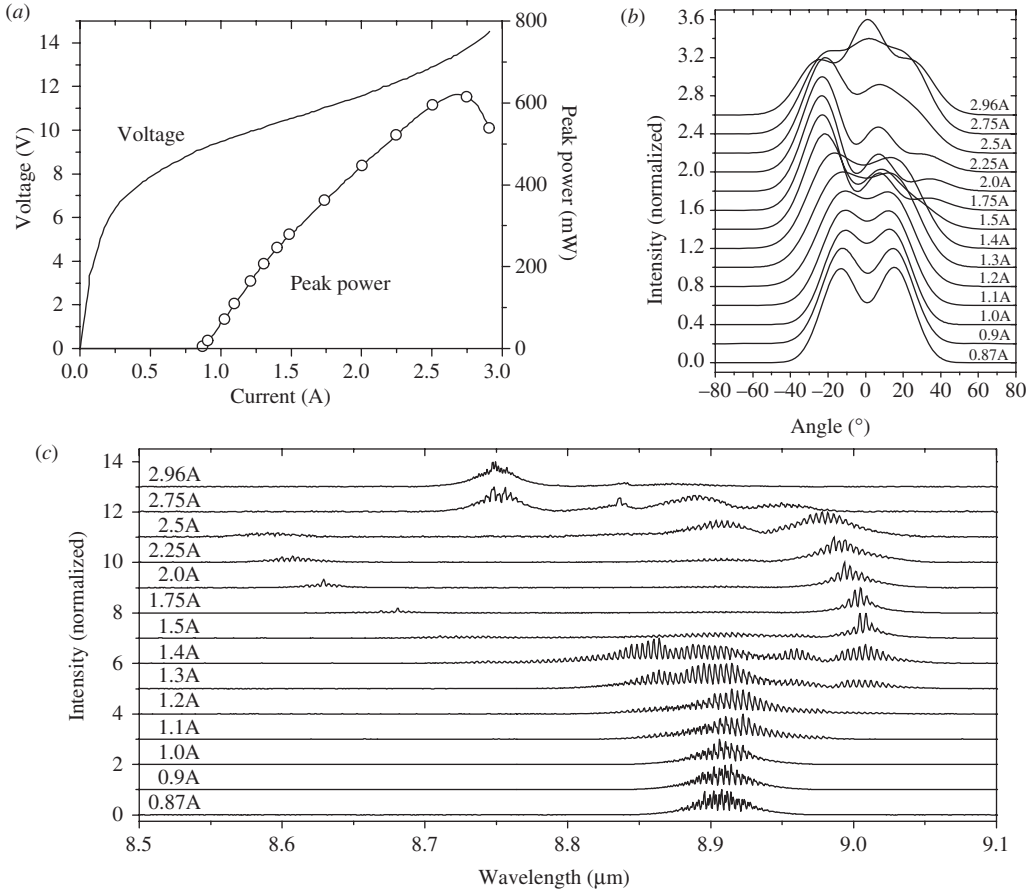

Figure 11. Hamamatsu QCL, with with $\lambda \approx 8.9\,\mu$m and an active region 19.4 μm wide.

which corresponds to a buried-heterostructure laser fabricated by Hamamatsu, with an active region width of 19.4 μm. Starting from threshold, this laser operates at three lateral modes TM_{00}, TM_{01}, and TM_{02}, and its far field is well described by an incoherent addition of modal intensities. The spectrum consists of at least three distinct combs of longitudinal modes, each comb belonging to a different lateral mode. At about 1.5 A, both the spectrum and the far field undergo a drastic change. The spectral combs merge into a single comb (Figure 11(*c*)), as if only one lateral mode is present. This locking of lateral modes is verified by Fourier analysis of the spectra below and above the bifurcation value of the current. At the same time, the far-field pattern becomes very asymmetric and shifts by about 30° off the waveguide axis (Figure 11(*b*)). This far field indicates the presence of all three lateral modes. Moreover, it can only be fitted by a *coherent* addition of the fields of all three lateral modes with fixed mutual phases. The beam steering is unlikely to originate from the thermal lens effect for two reasons. First, all heating-related effects are expected to be small because the laser operated in the pulsed regime with a low duty cycle. Second the changes in the beam pattern correlated with the spectral changes. In the case of thermal lensing, one should not expect to see strong changes in the spectrum.

This frequency-synchronized, phase-coherent behavior persists over a wide range of currents and is reproducible. Then at about 2.75 A, the laser undergoes the transition back to a state with several distinct spectral combs and symmetric far-field pattern.

Another buried heterostructure laser (from Agilent) showing a beam steering effect and phase locking is shown in Figure 12. The device lases at a wavelength $\lambda \approx 8.45$ μm and has an active region 11.2 μm wide. The LIV curve, far-field measurements and spectral dependence on injection current are presented in Figure 12. The laser is operated at room temperature in a pulsed regime, with a 80 kHz repetition rate. The pulse duration is 125 ns. The experimental conditions and setup are the same as the ones described in [10].

The laser beam shows asymmetry for currents between 1.25 and 2.1 A. Above this current, the laser enters into a roll-over region. The beam steering region of currents correlates with the frequency and phase locking region, although the combs remain distinct as

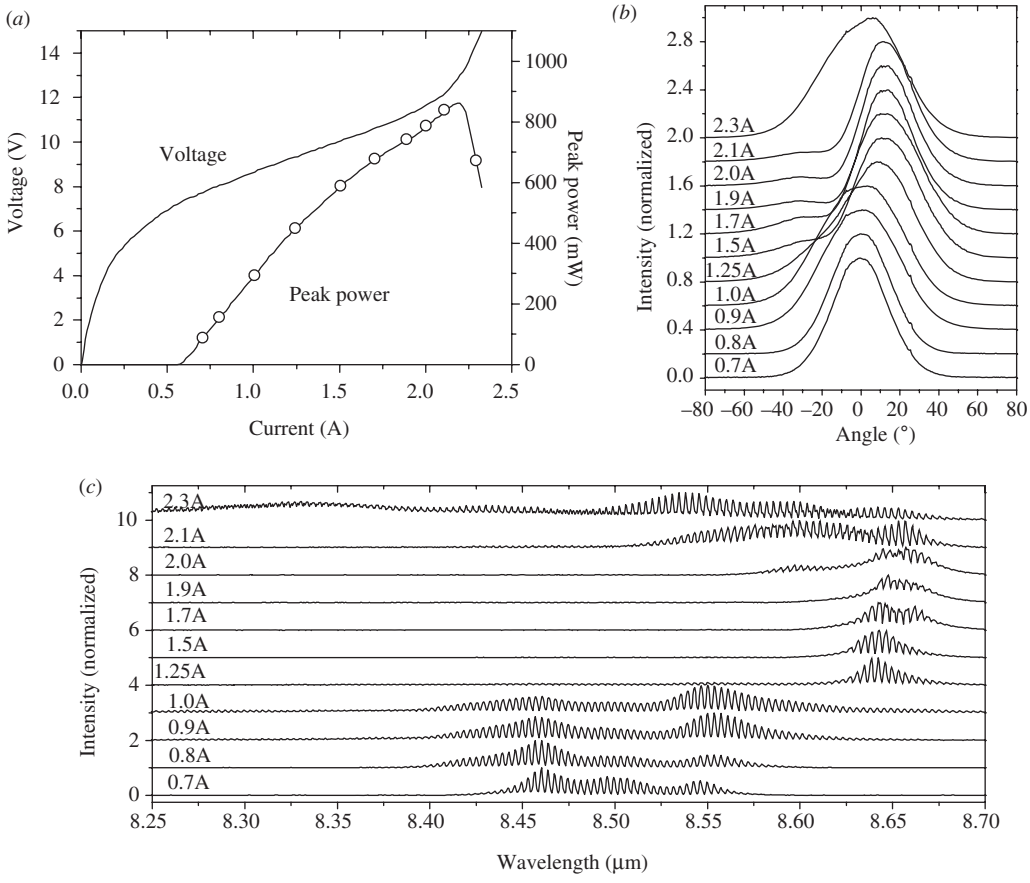

Figure 12. Agilent QCL, with $\lambda \approx 8.45$ μm and an active region 11.2 μm wide.

revealed by the Fourier analysis, similarly to the case studied in [10].

We emphasize that the existence of the phase-locked regime within a certain range of currents is not a unique property of one peculiar laser device. We observed the same behavior in many devices of different wavelengths and waveguide widths, fabricated by different manufacturers. The only common property was that all devices were of buried heterostructure type, with the active stripe overgrown by thick low-loss dielectric cladding. This design gives rise to very similar losses for several lateral modes. In fact, most of the devices started lasing at a higher-order lateral mode. In comparison, in the recent study of broad-ridge QCLs with lossy metal sidewalls [18], multi-lateral mode operation was readily observed, but no indication of phase coherence was found.

5. Conclusions

A model for the dynamics of transverse modes in QCLs has been derived and solved numerically. The numerical analysis predicted stable mode locking of three transverse modes through four-wave mixing interaction mediated by inhomogeneous saturation of the active region (spatial hole burning). The modes experience frequency pulling and lock to a single frequency, with a constant phase difference between them. We confirmed the results experimentally in a number of buried heterostructure QCLs.

For low level of the amplitude and phase fluctuations, there may exist two stable phase-locked states. This bistability regime would manifest itself by the presence of two separate combs in time-averaged measurements or as large intensity and spectral fluctuations in time-resolved data. In the pulsed regime, one could observe strong pulse-to-pulse fluctuations in laser intensity and spectra, which, however, would also require time-resolved measurements. We are not aware of any experimental confirmation of bistability in QCLs.

The phase coupling of transverse modes can be affected and controlled by selective inhomogeneous current injection or by selective modulation of modal losses through the fabrication of metallic structure on top of the laser waveguide. This could lead to the development of integrated mid-infrared sources with complex beam phase structure or to the generation of ultrashort pulses.

Acknowledgements

This work was supported in part by NSF Grants ECS-0547019 (CAREER), EEC-0540832 (MIRTHE ERC), and ECCS-0925446.

References

[1] Lugiato, L.A.; Prati, F.; Narducci, L.M.; Ru, P.; Tredicce, J.R.; Bandy, D.K. *Phys. Rev. A* **1988,** *37,* 3847–3866.

[2] Kaige, W.; Abraham, N.B.; Lugiato, L.A. *Phys. Rev. A* **1993,** *47,* 1263–1273.

[3] Aandrews, D.L. *Structured Light and Its Applications: An Introduction to Phase-Structured Beams and Nanoscale Optical Forces*; Academic Press: Amsterdam, 2008.

[4] Brambilla, M.; Cattaneo, M.; Lugiato, L.A.; Pirovano, R.; Prati, F.; Kent, A.J.; Oppo, G.L.; Coates, A.B.; Weiss, C.O.; Green, C.; D'Angelo, E.J.; Tredicce, J.R. *Phys. Rev. A* **1994,** *49,* 1427–1451.

[5] Denz, C.; Jander, P.; Schwab, M.; Sandfuchs, O.; Belić, M.; Kaiser, F. *Ann. Phys.* **2004,** *13,* 391–402.

[6] Mandel, P.; Tlidi, M. *J. Opt. B: Quantum Semiclass. Opt.* **2004,** *6,* R60–R75.

[7] Abraham, N.B.; Firth, W.J. *J. Opt. Soc. Am. B* **1990,** *7,* 951–962.

[8] Bewley, W.; Lindle, J.; Kim, C.S.; Vurgaftman, I.; Meyer, J.R.; Evans, A.J.; Yu, J.S.; Slivken, S.; Razeghi, M. *IEEE J. Quantum Electron.* **2005,** *41,* 833–841.

[9] Hinkov, B.; Fuchs, F.; Bronner, W.; Kohler, K.; Wagner, J. *IEEE J. Quantum Electron.* **2008,** *44,* 1124–1128.

[10] Yu, N.; Diehl, L.; Cubukcu, E.; Bour, D.; Corzine, S.; Zhu, J.; Höfler, G.; Wójcik, A.; Crozier, K.; Belyanin, A.; Capasso, F. *Phys. Rev. Lett.* **2009,** *102,* 013901.

[11] Yu, N.; Blanchard, R.; Fan, J.; Wang, Q.J.; Pflugl, C.; Diehl, L.; Edamura, T.; Furuta, S.; Yamanishi, M.; Kan, H.; Capasso, F. *IEEE Trans. Nanotechnol.* **2010,** *9,* 11–29.

[12] Lang, R. *IEEE J. Quantum Electron.* **1979,** *QE-15,* 718–726.

[13] Choi, H.; Norris, T.B.; Gresch, T.; Giovannini, M.; Faist, J.; Diehl, L.; Capasso, F. *Appl. Phys. Lett.* **2008,** *92,* 122114.

[14] Khanin, Y. *Principles of Laser Dynamics*; Elsevier: Amsterdam, 1995.

[15] Rana, F.; Ram, R.J. *Phys. Rev, B* **2002,** *65,* 125313.

[16] Gensty, T.; Elsäßer, W.; Mann, C. *Opt. Express* **2005,** *13,* 2032–2039.

[17] Yu, N.; Diehl, L.; Cubukcu, E.; Pflügl, C.; Bour, D.; Corzine, S.; Zhu, J.; Höfler, G.; Crozier, K.B.; Capasso, F. *Opt. Express* **2007,** *15,* 13227–13235.

[18] Stelmakh, N.; Vasilyev, M.; Toor, F.; Gmachl, C. *Appl. Phys. Lett.* **2009,** *94,* 013501.